Journal of Solid State Chemistry **152,** 492–502 (2000)
doi:10.1006/jssc.2000.8718, available online at http://www.idealibrary.com on IDEAL®

Synthesis and Characterization of New Phases: $Sr_{3.75}K_{1.75}Bi_3O_{12}$ and $Sr_{3.1}Na_{2.9}Bi_3O_{12}$

J. S. Pshirkov, S. M. Kazakov, A. M. Abakumov, S. N. Putilin, and E. V. Antipov[1]

Department of Chemistry, Moscow State University, Moscow 119899, Russia

C. Bougerol-Chaillout

Laboratoire de Cristallographie, CNRS-UJF, BP 166, 38042 Grenoble Cedex 9, France

and

O. I. Lebedev[2] and G. Van Tendeloo

EMAT, University of Antwerp (RUCA), Groenenborgerlaan 171, B-2020 Antwerp, Belgium

Received October 20, 1999; in revised form March 14, 2000; accepted March 16, 2000

New hexagonal phases were found in the Sr–K(Na)–Bi–O systems and characterized by X-ray powder diffraction, electron diffraction, and high-resolution electron microscopy (HREM). The crystal structures of $Sr_{3.75}K_{1.75}Bi_3O_{12}$ (space group $P\bar{6}2m$, $a = 10.4434(1)$ Å, $c = 3.37932(4)$ Å, $R_I = 0.019$, $R_P = 0.055$) and $Sr_{3.1}Na_{2.9}Bi_3O_{12}$ (space group $P\bar{6}2m$, $a = 10.1102(4)$ Å, $c = 3.3389(1)$ Å, $R_I = 0.024$, $R_P = 0.070$) were refined using X-ray powder data. The structures consist of chains of BiO_6 octahedra linked by the common edges whereas A cations occupy the interstices between the chains. This structure can be considered as the end member of the new $(Sr, K)_{6n+2}Bi_{3n-3}O_{12n}$ homologous series found by electron microscopy. The homologues with $n = 4$, 5, and 6 were observed, and their structures were deduced from HREM observations. © 2000 Academic Press

1. INTRODUCTION

The discovery of superconductivity in Bi-based perovskite oxides has attracted significant attention to these compounds. Pioneering works by Sleight *et al.* ($BaPb_{0.75}Bi_{0.25}O_3$, $T_c = 12$ K) (1) and Mattheis *et al.* (2) and later by Cava *et al.* ($K_{0.4}Ba_{0.6}BiO_3$, $T_c = 30$ K) (3) have inspired the further search for new superconductors among Bi-based oxides (4, 5). More recently, Kazakov *et al.* ($K_{0.6}Sr_{0.4}BiO_3$, $T_c = 12$ K) (6) and Khasanova *et al.* ($K_{0.9}Bi_{1.1}O_3$, $T_c = 10$ K and $La_{0.2}K_{0.8}BiO_3$, $T_c = 12$ K) (7, 8) have discovered new Bi-containing superconducting perovskites with similar structures possessing a three-dimensional framework of BiO_6 octahedra. Unfortunately, the three-dimensional character of the perovskite structure (ABO_3) significantly limits the number of Bi-based mixed oxides, which could be synthesized. In this case one can vary only the A-type cations, keeping intact Bi–O network. Contrarily, the 2D character of the layered copper-based high-T_c oxides favors a larger number of different structures with a variety of distinct compositions of insulating slabs alternating with conducting blocks along a long axis. Therefore, decreasing the dimensionality to 2D in the case of the bismuthates could be a promising way to obtain new phases.

Layered oxides of general composition $Ba_{n+1}(Pb, Bi)_nO_{3n+1}$ were first reported by Fu *et al.* (9). The structures of these tetragonal Ruddlesden–Popper-type phases consist of an alternate stacking along the c axis of perovskite and rock salt-type blocks. The electrical conductivity for pure Pb-based compounds increases with increasing n and the resistivity behavior changes from semiconductor-(Ba_2PbO_4) to metal-like ($Ba_4Pb_3O_{10}$). But, whereas superconductivity has been found in the solid solution $BaPb_{1-x}Bi_xO_3$ ($0 < x < 0.3$), no superconducting transition was observed for $Ba_4(Pb_{1-x}Bi_x)_3O_{10}$ ($0 < x < 0.3$). Furthermore, increasing the Bi content resulted in an increase of the resistivity (9–11). Contrary to the lead–bismuth layered oxides, only the second member ($A_3B_2O_7$) and the last member (ABO_3, simple perovskite) have been obtained for pure Bi-containing compounds. The

[1] To whom correspondence should be addressed. E-mail: antipov@icr.chem.msu.ru.

[2] On leave from Institute of Crystallography, RAS, Leninsky Prospekt 59, 117333 Moscow, Russia.

0022-4596/00 $35.00

second member of the Ruddlesden–Popper family $Ba_{1.7}K_{1.3}Bi_2O_7$ has been synthesized by Cava (12) and more recently by our group ($Sr_{1.6}K_{1.4}Bi_2O_7$) (13). Unfortunately, all attempts to induce superconductivity in these compounds were unsuccessful. This may be due to an inappropriate carrier concentration, which is considered to be too high for the occurrence of superconductivity. The valence of Bi in $Ba_{1.7}K_{1.3}Bi_2O_7$ is $+4.65$, while optimum for superconductivity is $+4.3$–4.4 for Ba-containing superconducting perovskites (14). Electronic band structure calculations for the $Ba_{1+x}K_{2-x}Bi_2O_7$ solid solution performed by Mattheiss showed that a slight decrease of the Bi valence could provide more favorable conditions for superconductivity in this material (15). However, despite numerous efforts, the Ba/K and Sr/K cation ratio remained constant whatever synthesis conditions were applied (12, 13).

Our attempts to synthesize the first member of the Ruddlesden–Popper series in the Sr–K–Bi–O system led to the formation of a new nonstoichiometric hexagonal phase rather than a phase with the K_2NiF_4 type structure. We present here the structural investigations of these new phases found in the Sr–K–Bi–O and Sr–Na–Bi–O systems.

2. EXPERIMENTAL PROCEDURES

The samples were synthesized by annealing under high oxygen pressure or in oxygen flow. First, $Sr_2Bi_2O_5$ was prepared by mixing $SrCO_3$ (Aldrich, $>99\%$) with Bi_2O_3 (Aldrich, 99.9%) and annealing the resulting powder at 700, 800, and 850°C for 100 h with several intermediate grindings. Appropriate amounts of $Sr_2Bi_2O_5$, KO_2 (96%), Na_2O_2 (95%), and Bi_2O_3 were mixed in a drybox filled with argon. The samples with initial compositions $Sr_{1+x}K_{1-x}BiO_y$ ($x = 0$, 0.33, 0.5), $Sr_{2.2}K_{0.5}BiO_y$, $Sr_{2.2}KBiO_y$, $Sr_{1.75}K_{0.5}BiO_y$, $Sr_{1.75}KBiO_y$, and $SrNa_{1+x}BiO_y$ ($x = 0.0$, 0.2, 0.5) were annealed under high oxygen pressure $p(O_2) = 40$–50 bar in a steel autoclave at 400–500°C for 20–60 h. The sample with the $SrKBiO_y$ initial composition was also obtained by annealing at 450°C for 24 h in oxygen flow.

X-ray powder diffraction (XRD) experiments were carried out with a focusing FR-552 Guinier camera (Cu$K\alpha_1$ radiation, $\alpha = 1.5406$ Å; Ge was used as an internal standard) or on STADI-P diffractometer (Cu$K\alpha_1$ radiation, curved Ge monochromator, transmission mode, scintillation counter). Adhesive tape was used as a supporting material for powdered samples. It has a broad halo in the 2θ range 10–30°. X-ray powder patterns for structure calculations were collected on thin mylar film, which does not exhibit such feature.

Electron diffraction (ED) and high-resolution electron microscopy (HREM) studies were performed using a JEOL 400EX instrument. EDX analysis and electron diffraction were performed using a Philips CM20 microscope with an attached LINK-2000 detector and a CM300 microscope with a Kevex detector. Image simulations were made by MacTempas software.

3. RESULTS

3.1. Synthesis and X-Ray Powder Diffraction Study

XRD revealed the formation of new phases (denoted to as H1) in the Sr–K–Bi–O and Sr–Na–Bi–O systems. The XRD patterns of H1 phases were indexed in the hexagonal unit cell with lattice parameters: $a = 10.4426(3)$ Å, $c = 3.3790(1)$ Å for the K-containing compound and $a = 10.1092(4)$ Å, $c = 3.3389(1)$ Å for the Na-containing one. The XRD pattern of K-containing H1 phase is shown in Fig. 1a.

We found that this phase was easily formed by annealing at 450°C for 24 h in oxygen flow of the $SrKBiO_y$ initial mixture. Furthermore, this phase has been prepared in pure form only in oxygen flow, while the high oxygen pressure technique favored the synthesis of a multiphase sample containing either a mixture of the H1 phase and the

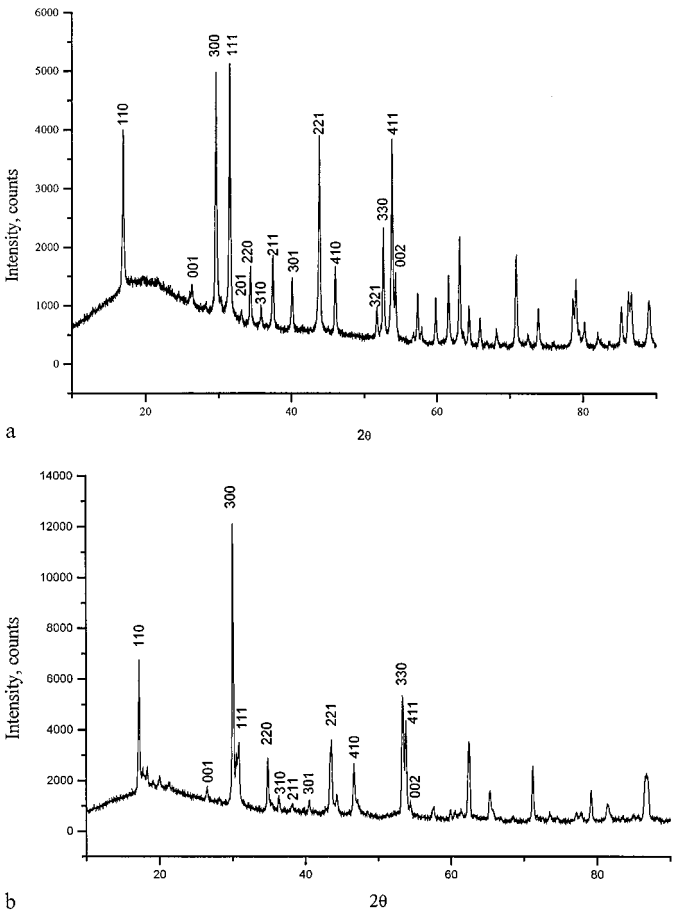

FIG. 1. X-ray diffraction patterns of the samples with nominal compositions: (a) $SrKBiO_y$; (b) $Sr_{1.5}K_{0.5}BiO_y$.

$Sr_{1.6}K_{1.4}Bi_2O_7$ layered one or another new hexagonal phase (referred to as H2).

The temperature of the synthesis strongly influences the final product of the reaction. Annealing of the $SrKBiO_y$ initial mixture performed at 400°C under 40 bar of oxygen partial pressure resulted in the formation of a multiphase sample with the hexagonal phase (H1) as the main phase and the layered $Sr_{1.6}K_{1.4}Bi_2O_7$ phase as an impurity. By increasing the synthesis temperature up to 450°C and by keeping the same pressure, the formation of the H1 phase was suppressed and the H2 phase was obtained.

The best sample of the H2 phase was obtained using $Sr_{1.5}K_{0.5}BiO_y$ as the starting composition and annealing at 450°C and $p(O_2) = 40$ bar for 22 h. An increase of the (Sr + K)/Bi ratio within the range 2–3.2 led to the appearance of Sr_3BiO_x as an impurity phase. The XRD pattern of H2 was indexed in a hexagonal unit cell with lattice parameters $a = 10.287(1)$ Å, $c = 3.520(4)$ Å (Fig. 1b). We were able to index only the main (subcell) reflections. Weak unindexed reflections were also found, which could originate from a decrease of the symmetry or from an increase of the cell dimensions for this compound. Indeed further electron microscopy study revealed the superstructure cell with significantly enlarged c parameter (see further). The synthesis conditions and the lattice parameters of the new H1 and H2 phases are summarized in Table 1.

The positions of the main peaks in the XRD patterns of the H1 and the H2 phases are similar; however, the intensities of the peaks in both cases are rather different. The reflections with $l = 0$ remain sharp on both XRD patterns, while in the case of the H2 phase the other reflections exhibit a broadening and a decrease of the intensity. This may suggest that in the case of H2 a well-established order exists in the a–b plane but a strong disorder appears along the c axis, as was revealed by electron microscopy study. More detailed investigation of this phase revealed much larger complexity than was expected at the first glance. Actually, several members of a new homologous series were detected by electron microscopy.

TABLE 1
Synthesis Conditions and Lattice Parameters of New Hexagonal Phases

Initial composition	Treatment conditions	Lattice parameters
	H1 phase	
$SrKBiO_y$	450°C, O_2 flow, 24 h	Hexagonal phase H1 $a = 10.4426(3)$ Å $c = 3.3790(1)$ Å
$SrNa_{1.2}BiO_y$	450°C, 40 bar O_2, 48 h	Hexagonal phase H1 $a = 10.1092(4)$ Å $c = 3.3389(1)$ Å
	H2 phase	
$Sr_{1.33}K_{0.67}BiO_y$	450°C, 40 bar O_2, 22 h	Hexagonal phase H2 $a = 10.3053(6)$ Å $c = 3.4990(6)$ Å
$Sr_{1.5}K_{0.5}BiO_y$	450°C, 40 bar O_2, 22 h	Hexagonal phase H2 $a = 10.287(1)$ Å $c = 3.520(4)$ Å
$Sr_{1.75}K_{0.5}BiO_y$	450°C, 40 bar O_2, 22 h	Hexagonal phase H2 $a = 10.292(1)$ Å $c = 3.509(1)$ Å

The hexagonal Na-containing H1 phase was obtained only by the high oxygen pressure technique. Contrary to the K-based phases, the Na-containing H1 phase does not form during the synthesis in oxygen flow. When the Na content was varied ($x = 0.0$, 0.2, 0.5), the pure H1 phase was only obtained when $SrNa_{1.2}BiO_y$ was used as the starting composition at 450°C under an oxygen pressure of 40 bar for 48 h. The increase of the annealing temperature to 500°C and annealing up to 48 h resulted in the formation of Na_3BiO_4 as an impurity. Further annealing for 24 h at 500°C led to the appearance of $Sr_{0.19}Bi_{0.81}O_{1.4}$ as an impurity due to Na evaporation. Pressure variation from 20 to 50 bar did not affect the phase purity. In comparison with the K-containing system, no other hexagonal phases such as H2 were observed.

3.2. *Crystal Structures of the H1 Phases*

3.2.1. Sr–K–Bi–O System. The crystal structure refinement of the H1 phase was performed on a single-phase sample of nominal composition $SrKBiO_y$ prepared by annealing in oxygen flow.

Since no extinction conditions were found from either ED or XRD patterns, $P\bar{6}2m$ and $P321$ were firstly chosen for structure simulations. The initial structure model was deduced from the analysis of probable cation distribution in the unit cell, and refinement based on this model gave reasonable results. A search for similar structures in the ICSD (16) database revealed two compounds Ca_2IrO_4 and $Ca_{4.74}Ir_3O_{12}$ with similar lattice geometry and atomic coordinates. In the structure of Ca_2IrO_4, A cations occupy three independent positions [denoted as M1, 1a; M2, 2c; and M3, 3g (position notations belong to the $P\bar{6}2m$ space group)] (17), while in the structure of $Ca_{4.74}Ir_3O_{12}$ only two of these positions (M2 and M3) are filled with A cations (18). All attempts to prepare the stoichiometric Ca_2IrO_4 phase performed in (18) were unsuccessful. The X-ray patterns of samples with a Ca to Ir ratio 8 : 6 showed impurities of IrO_2, while the pattern of sample with a Ca/Ir = 12 : 6 composition showed CaO remaining. The neutron refinement performed on the purest sample with a Ca/Ir = 9 : 6 composition revealed that this phase is indeed Ca-deficient, and the real composition is $Ca_{4.74}Ir_3O_{12}$. The cation position M1 at (0, 0, 0) was found to be empty and the M3 site was only partially occupied (g(Ca3) = 0.92).

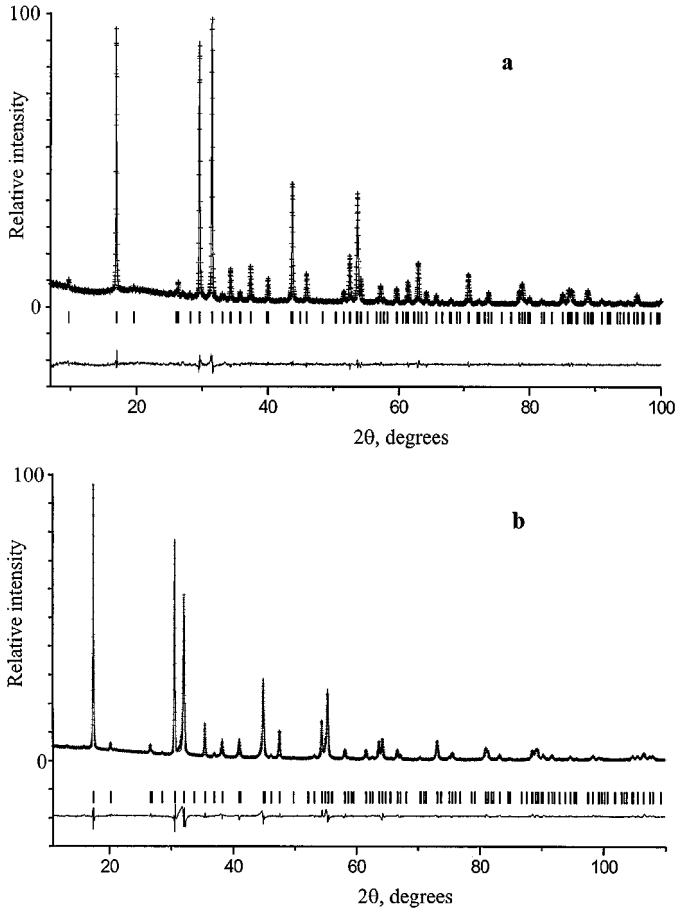

FIG. 2. Observed, experimental, and difference X-ray profiles for (a) $Sr_{3.75}K_{1.75}Bi_3O_{12}$ and (b) $Sr_{3.1}Na_{2.9}Bi_3O_{12}$ compounds.

For our refinement the atomic positions of $Ca_{4.74}Ir_3O_{12}$ were taken as initial ones. The refinement in the $P\bar{6}2m$ and $P321$ space groups yielded similar results, but in a latter case, the deviations of the z coordinate from 0 (for O2) and from 0.5 (for Sr2) were found to be within the range of standard deviations. Therefore the more symmetric $P\bar{6}2m$ group was chosen for the final refinement.

The structure refinement was performed using the RIETAN-97 program (19). The experimental, calculated and difference XRD profiles are shown in Fig. 2a. Crystallographic data collection parameters are presented in Table 2. The final structural information and the main interatomic distances are listed in Tables 3 and 4, respectively.

Considering that the two positions M2 and M3 are occupied by Sr and keeping M1 empty, the residual factor R_I was as low as 0.044. However, the difference Fourier map revealed a significant electron density peak in the M1 position, contrary to the $Ca_{4.74}Ir_3O_{12}$ structure. This peak indicates occupation of this site.

Subsequently, the electron densities at the M1, M2, and M3 positions were evaluated. All these positions were assumed to be occupied by Sr atoms only and their occupancy factors were refined with fixed thermal parameters $B = 1$ Å^2. The refined occupancies were found to be $g(M1) = 0.374(8)$, $g(M2) = 0.96(1)$, and $g(M3) = 0.714(9)$. From these data we concluded that the M2 position was fully occupied by Sr, whereas Sr, K, and possibly cation vacancies randomly occupied the M1 and M3 positions. Further refinements was performed assuming the same Sr/K ratio in the M1 and M3 positions. We were forced to make this suggestion due to the impossibility to refine the cation concentration and the vacancy content in two independent positions simultaneously.

Since EDX analysis found a ratio of Sr/K = 2.3 (the cation composition was found to be Sr/K/Bi = 0.94(2): 0.41(9): 1.00(8)), we used only the approximate value

TABLE 2
Crystallographic Data and Experimental Parameters for $Sr_{3.75}K_{1.75}Bi_3O_{12}$ and $Sr_{3.1}Na_{2.9}Bi_3O_{12}$

	$Sr_{3.75}K_{1.75}Bi_3O_{12}$	$Sr_{3.1}Na_{2.9}Bi_3O_{12}$
Space group	$P\bar{6}2m$	$P\bar{6}2m$
Lattice parameters (Å)	$a = 10.4434(1)$	$a = 10.1102(4)$
	$c = 3.37932(4)$	$c = 3.3389(1)$
Volume (Å^3)	319.189(7)	295.57(2)
Z	1	1
Calculated density, g/cm^3	6.326	6.501
Scan range, step (deg. 2θ)	7.0–100, 0.02	11–110, 0.01
No. of refined parameters	34	34
No. of reflections	92	99
R_{wP}, R_P, R_I	0.072, 0.055, 0.019	0.104, 0.070, 0.024

TABLE 3
Atomic Parameters for $Sr_{3.75}K_{1.75}Bi_3O_{12}$ (First Row) and $Sr_{3.1}Na_{2.9}Bi_3O_{12}$ (Second Row)

Atom	Position	x/a	y/b	z/c	B (Å^2)	g
M1 (0.5Sr + 0.5K)	1*a*	0	0	0	1.4(4)	0.5
M1 (0.95Na + 0.05Sr)					0.4(4)	1.0
M2 (Sr)	2*c*	$\frac{2}{3}$	$\frac{1}{3}$	$\frac{1}{2}$	0.7(2)	1.0
M2 (0.85Sr + 0.15Na)					0.9(2)	
M3 (0.5Sr + 0.5K)	3*g*	0.7000(5)	0	$\frac{1}{2}$	1.8(2)	1.0
M3 (0.55Na + 0.45Sr)		0.6942(6)			1.3(2)	
Bi	3*f*	0	0.3385(2)	0	0.20(3)	
Bi			0.3317(2)		0.58(2)	
O1	3*g*	0.472(2)	0	$\frac{1}{2}$	0.3(2)	
O1		0.443(2)			0.7(2)	
O2	6*j*	0.438(2)	0.222(1)	0	0.3(2)	
O2		0.453(2)	0.235(1)		0.7(2)	
O3	3*g*	0.197(2)	0	$\frac{1}{2}$	0.3(2)	
O3		0.188(2)			0.7(2)	

TABLE 4
Selected Interatomic Distances (Å) in $Sr_{3.75}K_{1.75}Bi_3O_{12}$ and $Sr_{3.1}Na_{2.9}Bi_3O_{12}$

	$Sr_{3.75}K_{1.75}Bi_3O_{12}$	$Sr_{3.1}Na_{2.9}Bi_3O_{12}$
M1–O3	2.66(1) × 6	2.53(1) × 6
M2–O1	3.028(6) × 3	2.975(3) × 3
M2–O2	2.67(1) × 6	2.51(1) × 6
⟨M2–O_{av}⟩	2.78(1)	2.67(1)
M3–O1	2.38(2) × 1	2.54(2) × 1
M3–O2	2.60(1) × 4	2.56(1) × 4
M3–O3	2.758(5) × 2	2.701(5) × 2
⟨M3–O_{av}⟩	2.61(1)	2.59(1)
Bi–O1	2.19(1) × 2	2.01(1) × 2
Bi–O2	2.01(1) × 2	2.059(9) × 2
Bi–O3	2.24(1) × 2	2.22(1) × 2
⟨Bi–O_{av}⟩	2.15(1)	2.10(1)

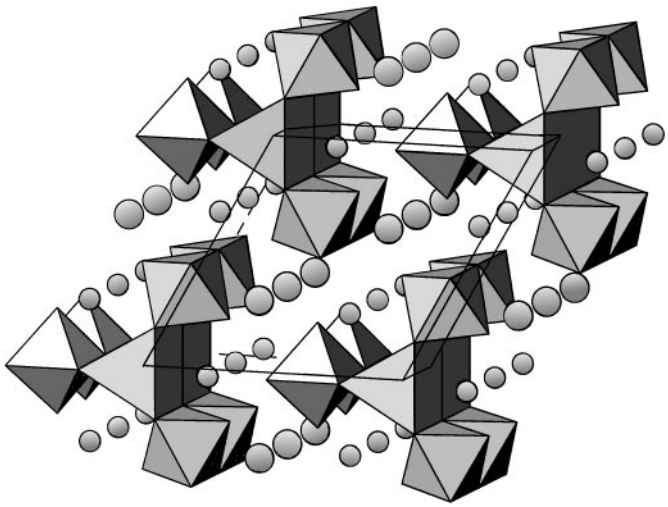

FIG. 3. Crystal structure of $Sr_{3.75}K_{1.75}Bi_3O_{12}$. Bi atoms are placed in the octahedra, and M1 atoms are placed in trigonal prisims. M2 and M3 atoms are imaged as large and small spheres, respectively.

Sr/K = 0.5/0.5 in these two positions, which were calculated assuming full occupancy of the M2 position by Sr atoms and taking into account the refined Sr occupancies as a first step of the calculations. At the final stage of the refinement, the thermal parameters were refined with fixed occupancy factors $g(M1) = 0.5$ and $g(M3) = 1.0$, and the results obtained are listed in Table 3. The chemical formula derived from the refined occupancies was $Sr_{3.75}K_{1.75}Bi_3O_{12}$. The formal valence of Bi calculated from this cation composition is close to $+5$ ($V_{Bi} = +4.92$), and it gives us indirect support that the refined values of the cation occupancies are reasonable. The evaporation of K from the starting mixture during the reaction in oxygen flow could be a reason of the observed deviation of the refined chemical composition from the starting cation ratio.

It should be noted that the refinement of the crystal structure with the M1 position occupied by K atoms only with $g(M1) = 0.75$ does not change the reliability factors, the atomic coordinates, the thermal parameters, or the interatomic distances. However, in this case the phase composition should be equal to $Sr_{3.5}K_{2.25}Bi_3O_{12}$, which strongly deviates from the experimental EDX results. We understand that the experimental facilities used cannot provide an unambiguous answer on the exact cation and vacancy distribution over the M1 and the M3 positions and the real chemical composition of this compound may slightly differ from the calculated one.

The crystal structure is shown in Fig. 3. It is made up of chains of edge-sharing BiO_6 octahedra running along the *c* direction. Three pairs of Bi–O distances are present: a short one at 2.01 Å and two longer ones at 2.19 and 2.24 Å. Alkaline-earth/alkali cations occupy three different positions between the chains. The M1 cations are in trigonal prisms (CN = 6). For the M3 and the M2 cations the coordination polyhedra are capped trigonal prisms (CN = 7) and tricapped trigonal prisms (CN = 9), respectively. In the capped trigonal prism, the M3 atom is displaced from the center toward a capped face. The polyhedra form edge-sharing chains of capped trigonal prisms and face-sharing chains of trigonal prisms and tricapped trigonal prisms.

3.2.2. Sr–Na–Bi–O System. In case of the Na-containing phase the refinement was performed on a sample of $SrNa_{1.2}BiO_y$ nominal composition using the $Ca_{4.74}Ir_3O_{12}$ structure as the initial model. We used the same approach as for the K-containing phase. However, according to the EDX analysis results [indicating a (Sr + Na)/Bi ratio close to 2] all cation positions would be fully occupied. We first refined occupancies of the *A* cation sites, assuming they are only occupied by Sr and fixing $B = 1$ Å^2. The results were $g(M1) = 0.319(8)$, $g(M2) = 0.89(1)$, and $g(M3) = 0.601(9)$. According to this calculation the following occupations were assigned: M1 = 0.95Na + 0.55Sr, M2 = 0.85Sr + 0.15Na, and M3 = 0.55Na + 0.45Sr. It should be noted that the scattering density in the M1 position is very close to the scattering power of pure Na. The refinement of the thermal factor at different Sr/Na ratios in this position revealed a strong correlation between these two parameters (for instance, $B = -0.9$ Å^2 at Sr/Na = 0.0/1.0 and $B = 1.6$ Å^2 at Sr/Na = 0.1/0.9). In the successive refinements the occupations of M1, M2, and M3 positions are kept fixed. The thermal parameters for the oxygen atoms were combined in one block and refined simultaneously. The final results are listed in Tables 2, 3, and 4. The experimental, calculated, and difference XRD profiles are shown in Fig. 2b. The refined chemical composition is written as $Sr_{3.1}Na_{2.9}Bi_3O_{12}$. The fact that the M1 site occupation is

higher for the Na-containing compound than for the K-containing one can be explained by the difference in synthesis conditions and ionic radii of alkali cations. The synthesis of the Na-based compound was performed in a closed vessel under oxygen pressure, thus diminishing the Na evaporation in contrast with the conditions for the synthesis of the K-containing compound (open vessel, oxygen flow).

It is necessary to mention that the analysis of the correlation matrix revealed a strong correlation ($> 60\%$) between the x coordinates of the O1 and O3 atoms for both $Sr_{3.1}Na_{2.9}Bi_3O_{12}$ and $Sr_{3.75}K_{1.75}Bi_3O_{12}$ structures. This fact decreases the accuracy of a simultaneous refinement of the O1 and O3 atomic coordinates and can be a possible source for discrepancies in the M3–O1 and Bi–O1 distances between Na- and K-containing H1 phases. Nevertheless, we suppose that the variation of the average interatomic distances approximately reflects the changes in the crystal structure on going from the $Sr_{3.75}K_{1.75}Bi_3O_{12}$ phase to the $Sr_{3.1}Na_{2.9}Bi_3O_{12}$ phase.

The crystal structure of the Na-containing H1 phase is close to that of the K-containing one. The lattice parameters tend to decrease when Na is introduced in the structure. The main difference is a shrinkage of the M–O distances (see average distances M–O in Table 4). This is in agreement with a decrease of the effective A cation radii in these sites. The M positions in the Na-containing phase are fully occupied in contrast to that of the K-containing phase. The Bi valence calculated from the refined cation composition for both compounds is close to $+5$, and this is an extra argument that the refined compositions are reasonable.

3.3. Electron Microscopy Study

Electron diffraction (ED) patterns of the K-containing H1 phase were obtained for the most relevant [0001] and [11$\bar{2}$0] zone axes (Fig. 4). The [0001] ED pattern clearly exhibits the 6-fold symmetry. Both patterns were completely indexed on a hexagonal unit cell with parameters $a \approx 10.4$ Å and $c \approx 3.4$ Å which are in a good agreement with that determined from X-ray diffraction (Table 1). No extinction conditions were found. ED patterns of Na-containing H1 phase exhibit no additional features (superstructure spots, stripes, and diffuse intensities) in comparison with the ED patterns of the K-based H1 phase. Unfortunately, the H1 compounds easily decompose under the electron beam irradiation at an elevated beam intensity, which hampers the HREM observation of the crystal structure.

The [0001] ED pattern of the H2 phase is very similar to that obtained for the H1 phase except for a small difference in the cell parameters. All reflections on this ED pattern are sharp and perfectly circular. In contrast to that, [11$\bar{2}$0] and [10$\bar{1}$0] ED patterns exhibit a significant difference in comparison with the corresponding patterns for the H1 phase

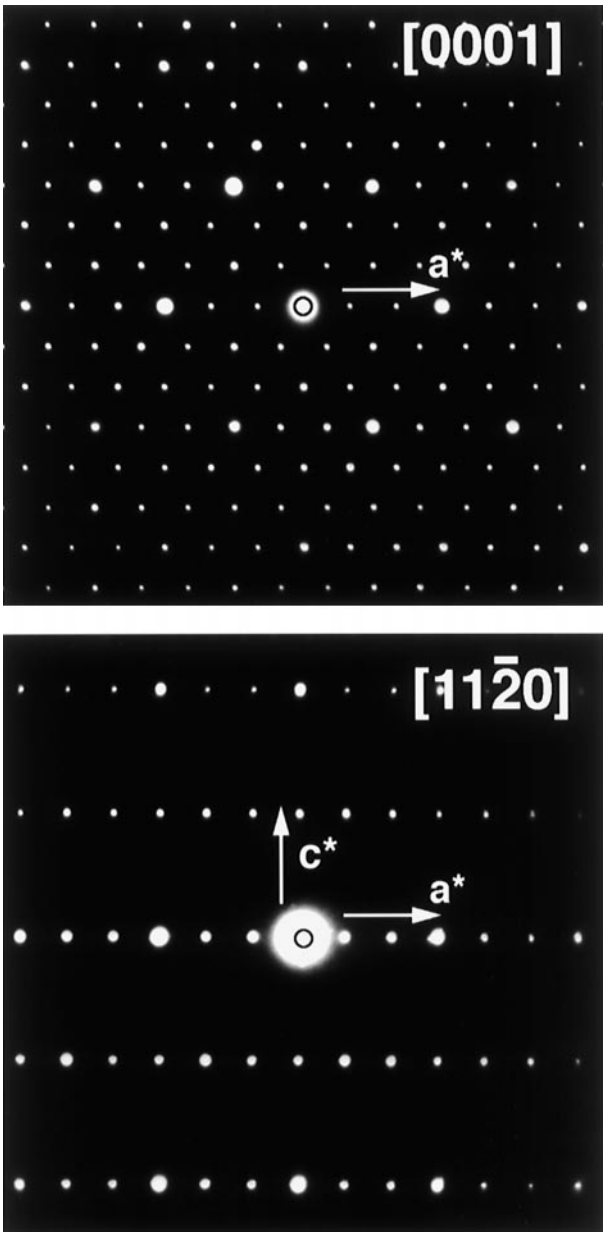

FIG. 4. ED patterns of the H1 phase ($Sr_{3.75}K_{1.75}Bi_3O_{12}$) along the [0001] and [11$\bar{2}$0] zone axis.

(Fig. 5). The brighter reflections on all patterns can be indexed with the cell parameters determined from X-ray diffraction for the H2 phase; they belong to the sublattice. All [11$\bar{2}$0] and [10$\bar{1}$0], however, contain superstructure reflections or diffuse intensity. Mostly, the diffuse intensity (Fig. 5a, b) indicates a large disorder along the c axis. In a number of cases regular superstructure spots were found (Fig. 5c, d). The superstructure spots are situated at $\frac{1}{6}$ of [0001] positions and the rows of superstructure reflections are oriented along the [000l] direction. ED patterns with superstructure spots at $\frac{1}{5}$ of [0001] and $\frac{1}{4}$ of [0001] positions

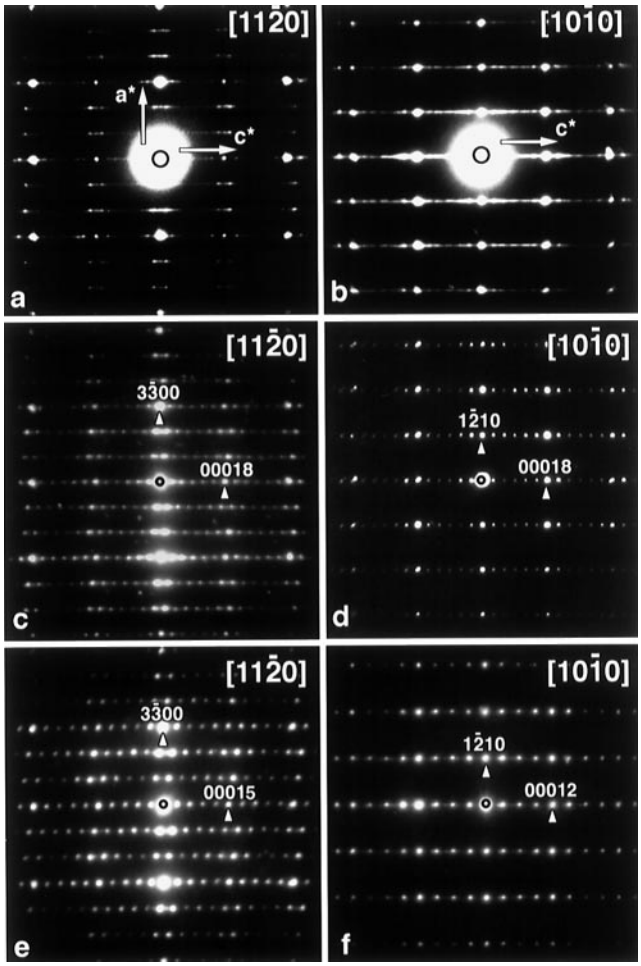

FIG. 5. [1 1 $\bar{2}$ 0] and [1 0 $\bar{1}$ 0] ED patterns of the H2 phase, with rows of diffuse intensity along [0001] (a, b) and with regular superstructure reflections placed at $\frac{1}{6}$ of [0001] (c, d), at $\frac{1}{5}$ of [0001] (e), and at $\frac{1}{4}$ of [0001] (f) positions.

were also occasionally observed (Fig. 5e, f). The [11$\bar{2}$0] ED pattern (Fig. 5c) exhibits a rhombohedral shift of the spot rows along c^* over $h \times \frac{1}{3}c^*$ resulting in the $-h + k + l = 3n$ extinction condition. Finally, the [11$\bar{2}$0] and [10$\bar{1}$0] ED patterns (Fig. 5c, d) of the ordered phase were indexed on an R-centered hexagonal lattice with parameters $a = 10.3$ Å and $c = 63.4$ Å.

The cation compositions of H1 and H2 phases were evaluated by EDX analysis. The EDX spectra were obtained from more than 20 different crystallites. The results of the measurement were averaged and produce Sr/K(Na)/Bi ratios equal to 0.94(2) : 0.41(9) : 1.00(8), 2.0(1):0.20(2):1.0(1), and 1.2(2):1.16(6):1.0(1) for the K-containing H1 and H2 phases and Na-containing H1 phase, respectively. It should be noted, however, that EDX also shows a strong inhomogeneity of the cation distribution in the samples. Therefore, the results of the quantitative analysis can only be considered as a rough estimation.

The [10$\bar{1}$0] HREM images of H2 compound reveal the formation of numerous stacking faults (Fig. 6a, b) with the fault planes parallel to (0001). The stacking faults have a width of one layer of bright dots and do not exhibit a side shift of the dot columns. An ordered array of stacking faults is shown in Fig. 6a. The fault planes are repeated every six layers; this repeat period is consistent with that observed in the ED pattern from Fig. 5d. The 6-layer stacking sequence is occasionally violated by the insertion of a thicker band of seven layers width as it is marked by a white arrow in Fig. 6a. To build a possible model of this superstructure, the atomic coordinates from the basic structure ($a = 10.4$ Å, $c = 3.3$ Å, space group $P\bar{6}2m$) were transformed into a new unit cell with parameters $a = 10.27$ Å and $c = 63.4$ Å. The space group was chosen as $R3$ because it is compatible with the crystal structure and does not exhibit extinction conditions besides the ones appearing from the centered lattice. Because the EDX analysis shows an excess of A cations in comparison with the ideal A_2BiO_4 composition and there is no possibility to accommodate the extra cations in the basic structure, it is reasonable to assume that the formation of the stacking faults is connected with the increase of Sr content. According to this assumption Bi cations were replaced by Sr cations in every sixth layer and appropriate atomic displacements were made to achieve reasonable interatomic Sr–O distances. The rhombohedral shift of the crystal structure over $\frac{1}{3}, \frac{2}{3}, \frac{1}{3}$ results in an unrealistically short Sr–Sr separation (1.7 Å) and part of the Sr atoms was

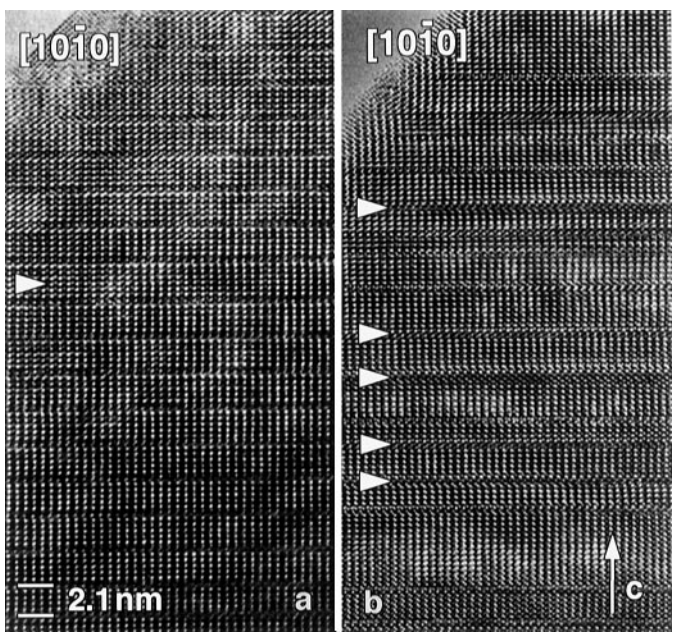

FIG. 6. [1 0 $\bar{1}$ 0] HREM images of the H2 phase. (a) Ordered 6-layer stacking sequence, occasionally an inserted 7-layer lamella is marked by an arrow; (b) disordered alternation of stacking faults and twin boundaries (marked by arrows).

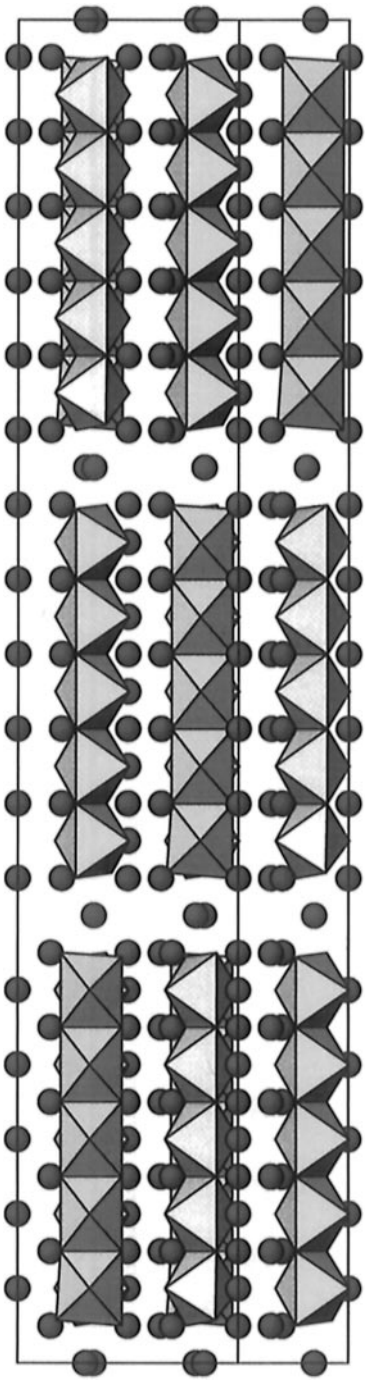

FIG. 7. Structure model of the 6-layer homologue based on HREM evidence (Fig. 6a). BiO_6 octahedra are shown, and (Sr, K) atoms are imaged as shaded spheres.

removed from the fault plane (Fig. 7). The $(Sr, K)_{2.53}BiO_4$ (or $(Sr, K)_{38}Bi_{15}O_{96}$) composition was calculated for this structure model; it is in agreement with the composition determined by EDX. The HREM images calculated using this model (Fig. 8) show good agreement with the experimental image shows in Fig. 6a. Using the same building principles the structure models for the compounds with one Sr-enriched layer per every 4 and 5 normal layers were constructed. The compositions deduced from these models are $(Sr, K)_{26}Bi_9O_{48}$ and $(Sr, K)_{32}Bi_{12}O_{60}$ for 4-layer and

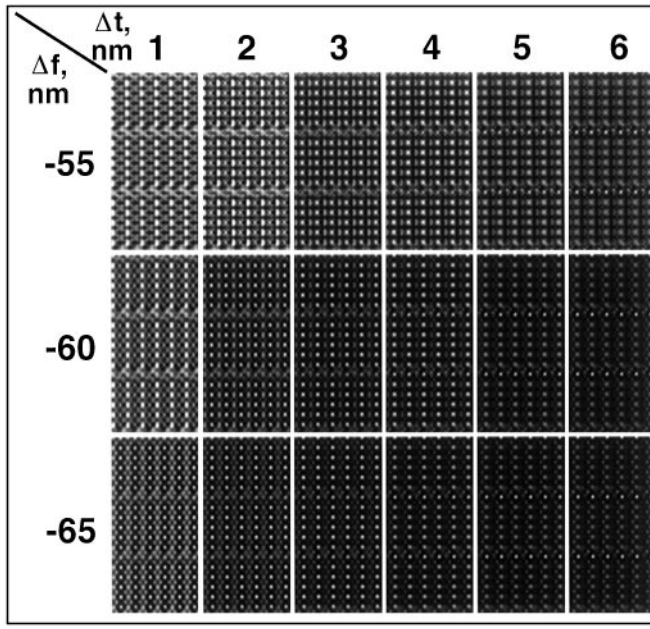

FIG. 8. Matrix of $[1\,0\,\bar{1}\,0]$ HREM images calculated using the structure model shown in Fig. 7.

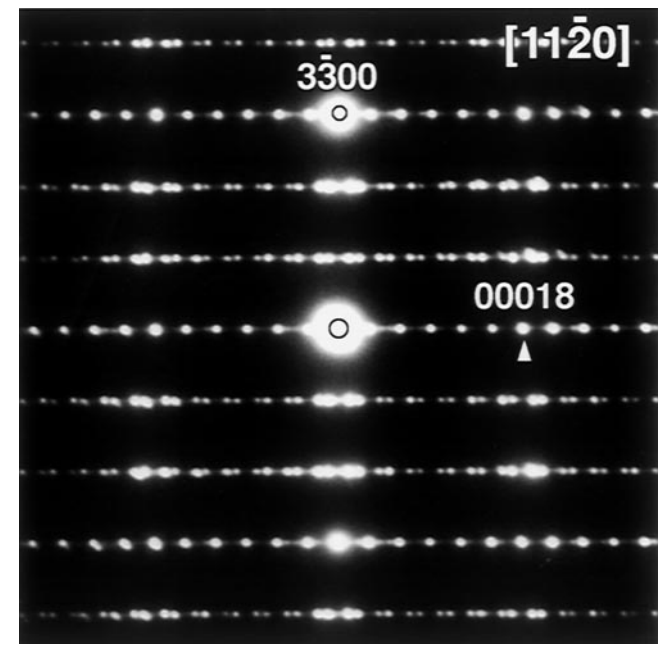

FIG. 9. $[1\,1\,\bar{2}\,0]$ ED pattern taken from a twinned region of 6-layer homologue. Note the splitting of spots in the $[1\,\bar{1}\,0\,l]$ and the $[2\,\bar{2}\,0\,l]$ rows. The central row and every third rows are unsplit.

5-layer homologues, respectively. Thus the common formula of the compounds belonging to this homologous series is $(Sr, K)_{6n+2}Bi_{3n-3}O_{12n}$.

Figure 6b reproduces the $[10\bar{1}0]$ HREM image corresponding to the ED pattern shown in Fig. 5b. The stacking faults are no longer equally spaced, which results in a banded structure of the crystallite with different widths of the bands. The computer-simulated Fourier transformation obtained from the the widest band shows the pattern corresponding to the ED pattern of the H1 phase. The computer image simulation of the basic structure was performed using the results of the Rietveld refinement of the K-containing H1 phase. The correspondence between calculated and experimental images was found to be satisfactory at $\Delta f = -60$ nm and $t = 4$ nm. In addition to the stacking faults discussed, a different type of planar defect resulting in a lateral shift of the bright dot columns over $\frac{1}{3}$ of the intercolumnar distance is also found (marked by arrows in Fig. 6b). These defects can be attributed to mirror microtwins, as will be shown below.

The $[11\bar{2}0]$ ED diffraction pattern of the 6-layer homologue with a clear splitting of reflections due to twinning is shown in Fig. 9. The unsplit reflections are in the $[000l]$ and $[3\bar{3}0l]$ rows whereas all reflections in the $[1\bar{1}0l]$ and $[2\bar{2}0l]$ rows are split, indicating the presence of mirror twins with a (0001) twin plane. The $[11\bar{2}0]$ HREM images of a single domain region and a twinned region of the 4-layers homologue are shown in Fig. 10a and b, respectively. The rhombohedral shift is observed in Fig. 10a by side displacement of the vertical rows of bright dots over $\frac{1}{3}$ $[1\bar{1}00]$. The twin domains can be distinguished by opposite directions of such displacement (more easily visible under grazing incidence in Fig. 10b). The simulated $[10\bar{1}0]$ and $[11\bar{2}0]$ HREM images (Fig. 11) of the twin boundary show good agreement with the contrast observed on the corresponding experimental HREM images (Figs. 6b and 10b). It should be noted that the columns of bright dots are shifted on the $[10\bar{1}0]$ calculated HREM image on passing across the twin boundary; this was also found experimentally (Fig. 6b).

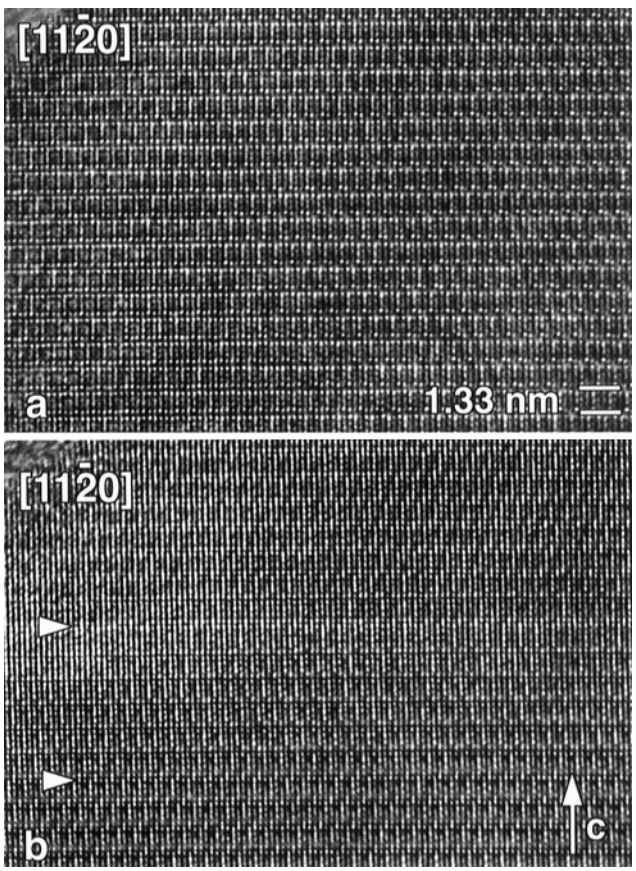

FIG. 10. $[1\,1\,\bar{2}\,0]$ HREM images of the 4-layer homologue showing (a) a region of perfect structure and (b) a region containing microtwins (twin boundaries are marked by arrows).

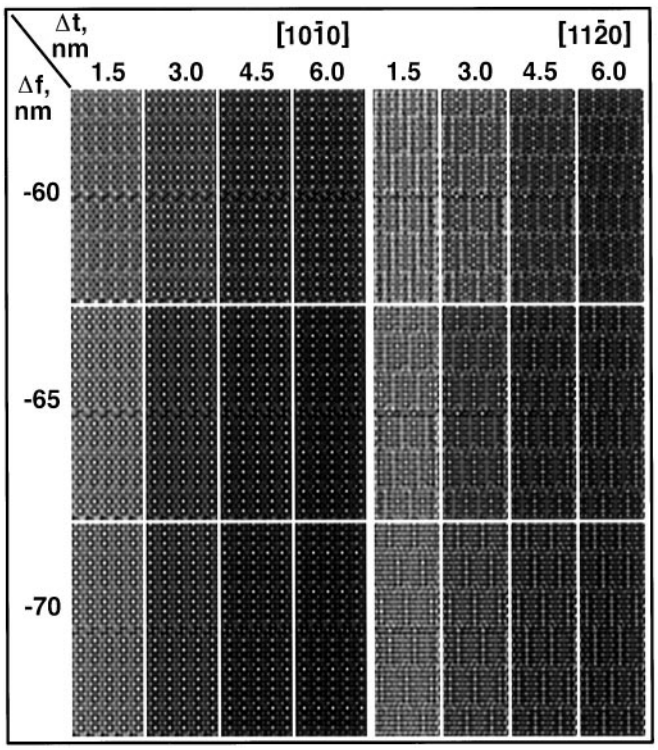

FIG. 11. Calculated $[1\,0\,\bar{1}\,0]$ and $[1\,1\,\bar{2}\,0]$ HREM images of the twin boundary (compare with Figs. 6b and 10b, respectively).

4. DISCUSSION

Mixed oxides with composition A_2BO_4 can belong to numerous structural types which differ one from another by the coordination of A and B cations as well as by the sharing scheme of coordination polyhedra, resulting in the formation of chains, layers, or three-dimensional frameworks. Among these complex oxides a family of compounds could

be separated whose structures are built up by BO_6 octahedra connected into the strings by edge sharing. All structures of the members of this family can be derived from the simplest parent structure of Sr_2PbO_4 (Fig. 12a) (20). It can be described by the layer sequence -(Sr_2O_2)-(PbO_2)-(Sr_2O_2) — alternating along the direction of the strings. The structure of Pb_3O_4 (Pb_2PbO_4) (Fig. 12b) also consists of the similar (Pb_2O_2) and (PbO_2) layers (21). The arrangements of the octahedra strings are the same for both structures, but the $Sr_2PbO_4 \rightarrow Pb_2PbO_4$ structure transition requires a 90° rotation of each second (Pb_2O_2) layer, resulting in a stacking sequence -(Pb_2O_2)-(PbO_2)-(Pb_2O_2)*-(PbO_2)-(Pb_2O_2)- and doubling the repeat period along the strings. A visual comparison of the projection in the *ab* plane of the $Ca_{4.74}Ir_3O_{12}$, H1, and Sr_2PbO_4 structures shows the close resemblance of these structures (Fig. 12c, d). The Sr_2PbO_4 orthorhombic unit cell marked by dashed lines in the $Ca_{4.74}Ir_3O_{12}$ and H1 structure projections outlines this similarity. $Ca_{4.74}Ir_3O_{12}$ is hexagonal due to the rotation of octahedron chains along the *c* axis and the ordered placement of Ca cations and cation vacancies situated in the trigonal channels at 0, 0, *z* position. The stacking sequence -($Ca_{5/3}\square_{1/3}O_2$)-(IrO_2)-($Ca_{5/3}\square_{1/3}O_2$)-is similar to that for Sr_2PbO_4; the (Sr_2O_2) and ($Ca_{5/3}\square_{1/3}O_2$) layers have close cation distribution and only differ by the anion arrangement. The trigonal channels, when are empty in the $Ca_{4.74}Ir_3O_{12}$ structure, are partially filled in the H1 structure by *A* cations. These cations occupy the *A* position in (BiO_2) layers resulting in the stacking sequence -($A_{5/3}\square_{1/3}O_2$)-($BiA_{1/3}O_2$)-($A_{5/3}\square_{1/3}O_2$)-. It should be noted that for the consideration described above the idealized stacking formulae for the $Ca_{4.74}Ir_3O_{12}$ and the H1

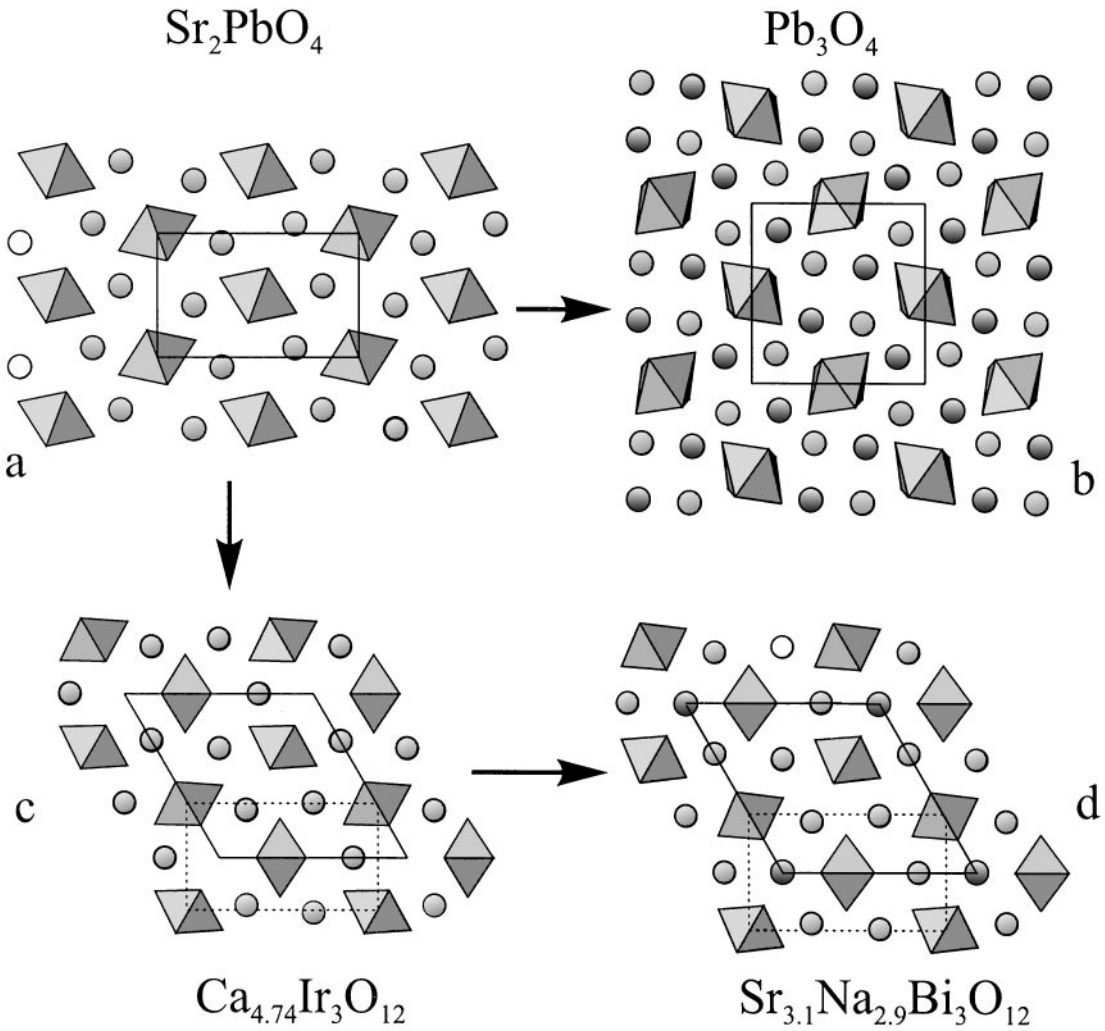

FIG. 12. Comparison between structure projections of (a) Sr_2PbO_4, (b) Pb_3O_4, (c) $Ca_{4.74}Ir_3O_{12}$, and (d) H1 phase. Shaded octahedra show the projections of the strings. The dashed lines represent the Sr_2PbO_4-type unit cell.

compounds were written without taking into account the random distribution of cation vacancies in A positions.

The comparison of the H1 hexagonal structure with the K_2NiF_4 layered structure shows that a change of the A cation results in a structural transformation. Several examples of such phase transformations are observed: $Ba_2PbO_4 \rightarrow Sr_2PbO_4$ (K_2NiF_4 to Sr_2PbO_4) (22) or Sr_2IrO_4 (distorted K_2NiF_4-type) $\rightarrow$ "Ca_2IrO_4" (the real composition is $Ca_{4.74}Ir_3O_{12}$) (23). The structural field map of A_2BO_4 compounds (24) allows us to conclude that the driving force causing such a transformation is a decrease of the A cation radius. The transformation from Sr_2PbO_4 to K_2NiF_4 is accompanied by a change of the octahedron connection scheme from edge sharing to corner sharing. We hope that increasing the A cation radius (for example, by using Rb or Ba) might lead to the formation of bismuthates with the K_2NiF_4-type structure, and this problem is currently under investigation.

The variation of the ratio between (Sr, K) and Bi cations resulted in the formation of a new homologous series based on the H1 structure. An increase of the content of A cations leads to the appearance of Sr-enriched layers, which can alternate in an ordered manner with blocks of the H1 parent structure. According to a possible model for the crystal structure proposed on the basis of HREM observations, the common idealized fomula for this homologous series can be written as $(Sr, K)_{6n+2}Bi_{3n-3}O_{12n}$. The presence of members of this homologous family with $n = 4$, 5, and 6 was revealed by electron diffraction and high-resolution electron microscopy. In this case the H1 phase could be considered as a finite member of this series with $n = \infty$. For Na-containing samples, superstructures related to the formation of a $(Sr, Na)_{6n+2}Bi_{3n-3}O_{12n}$ homologous series were never observed.

ACKNOWLEDGMENTS

A.A. and O.L. are grateful to DWTC and FWO (Belgium), respectively, for financial support during their stay at the University of Antwerp. This work was performed within the framework of IUAP 4/10 of the Belgian government and supported by PICS-RFBR (98-03-2207, 00-03-32472) and INTAS (1136) grants.

REFERENCES

1. A. W. Sleight, J. L. Gillson, and P. E. Bierstedt, *Solid State Commun.* **17,** 27 (1975).
2. L. F. Mattheiss, E. M. Gyorgy, and D. W. Johnson, Jr., *Phys. Rev. B* **37,** 3745 (1988).
3. R. J. Cava, B. Batlogg, J. J. Krajewski, R. Farrow, L. W. Rupp, Jr., A. E. White, K. Short, W. F. Peck, and T. Kometani, *Nature* (*London*) **332,** 814 (1988).
4. E. Wang, J.-M. Tarascon, and G. W. Hull, *Solid State Commun.* **74,** 471 (1990).
5. Z. Iqbal, G. H. Kwei, B. L. Ramakrishna, and E. W. Ong, *Physica C* **167,** 369 (1990).
6. S. M. Kazakov, C. Chaillout, P. Bordet, J. J. Capponi, M. Nunez-Regueiro, A. Rysak, J. L. Tholence, P. G. Radaelli, S. N. Putilin, and E. V. Antipov, *Nature* (*London*) **390,** 148 (1997).
7. N. R. Khasanova, A. Yamamoto, S. Tajima, X.-J. Wu, and K. Tanabe, *Physica C* **305,** 275 (1998).
8. N. R. Khasanova, F. Izumi, T. Kamiyama, K. Yoshida, A. Yamamoto, and S. Tajima, *J. Solid State Chem.* **144,** 205 (1999).
9. W. T. Fu, H. W. Zandbergen, Q. Xu, J. M. van Ruitenbeek, L. J. de Jongh, and G. Van Tendeloo, *Solid State Commun.* **70,** 1117 (1989).
10. Q. Xu, W. T. Fu., J. M. van Ruitenbeek, and L. J. de Jongh, *Physica C* **167,** 271 (1990).
11. Q. Xu, W. T. Fu, J. M. van Ruitenbeek, L. J. de Jongh, M. Drillon, and Y. Bruynseraede, *J. Less-Common Metals* **164–165,** 948 (1990).
12. R. J. Cava, T. Siegrist, W. F. Peck, Jr., J. J. Krajewski, B. Batlogg, and J. Rosamilia, *Phys. Rev. B* **44,** 9746 (1991).
13. J. S. Pshirkov, S. M. Kazakov, C. Bougerol-Chaillout, P. Bordet, J. J. Capponi, S. N. Putilin, and E. V. Antipov, *J. Solid State Chem.* **144,** 405 (1999).
14. Y. Idemoto, Y. Iwata, and K. Fueki, *Physica C* **201,** 43 (1992).
15. L. F. Mattheiss, *Phys. Rev. B* **45,** 12528 (1992).
16. ICSD/Retrieve 2.0.1, M. Brendt, 23 April 1996.
17. D. Babel, W. Rüdorff, and R. Tschöpp, *Z. Anorg. Allg. Chem.* **347,** 282 (1966).
18. F. J. J. Dijksma, J. F. Vante, E. Frikkee, and D. J. W. Ijdo, *Mater. Res. Bull.* **28,** 1146 (1993).
19. F. Izumi, *in* "The Rietveld Method," Chap. 13 (R. A. Young, ed.). Oxford University Press, Oxford, 1993.
20. M. Troemel, *Z. Anorg. Allg. Chem.* **371,** 237 (1969).
21. J. R. Cavarri, G. Calvarin, and D. Weigel, *J. Solid State Chem.* **14,** 91 (1975).
22. H. Stoll and R. Hoppe, *Z. Anorg. Allg. Chem.* **548,** 165 (1987).
23. Q. Huang, J. L. Soubeyroux, O. Chmaissem, I. Natali Sora, A. Santoro, R. J. Cava, J. J. Krajewski, and W. F. Peck, *J. Solid State Chem.* **112,** 355 (1994).
24. O. Muller and R. Roy, "The major ternary structural families," p. 76. Springer-Verlag, New York, 1974.